Research Paper

Experimental investigation of the biomechanics of urethral tissues and structures

Arturo Nicola Natali[1,2], Emanuele Luigi Carniel[1,2], Alessandro Frigo[1,2], Piero Giovanni Pavan[1,2], Silvia Todros[1,2], Paola Pachera[1,2], Chiara Giulia Fontanella[2,3], Alessandro Rubini[2,3], Laura Cavicchioli[4], Yochai Avital[5] and Giulia Maria De Benedictis[2,5]

[1]*Department of Industrial Engineering, University of Padova, Italy*
[2]*Centre for Mechanics of Biological Materials, University of Padova, Italy*
[3]*Department of Biomedical Sciences, University of Padova, Italy*
[4]*Department of Comparative Biomedicine and Food Science, University of Padova, Italy*
[5]*Department of Animal Medicine, Production and Health, University of Padova, Italy*

Experimental Physiology

New Findings

- **What is the central question of this study?**
  Prostheses for treatment of urinary incontinence elicit complications associated with an inadequate mechanical action. This investigation aimed to define a procedure addressed to urethral mechanical characterization. Experimental tests are the basis for constitutive formulation, with a view to numerical modelling for investigation of the interaction between the tissues and a prosthesis.
- **What is the main finding and its importance?**
  Horse urethra, selected for its histomorphometric similarity to human urethra, was characterized by integrated histological analysis and mechanical tests on the biological tissue and structure, leading to constitutive formulation. A non-linear, anisotropic and time-dependent response was found, representing a valid basis for development of a numerical model to interpret the functional behaviour of the urethra.

Urinary dysfunction can lead to incontinence, with an impact on the quality of life. Severe dysfunction can be overcome surgically by the use of an artificial urinary sphincter. Nonetheless, several complications may result from inappropriate functioning of the prosthesis, in many instances resulting from an unsuitable mechanical action of the device on the urethral tissues. Computational models allow investigation of the mechanical interaction between biological tissues and biomedical devices, representing a potential support for surgical practice and prosthesis design. The development of such computational tools requires experimental data on the mechanics of biological tissues and structures, which are rarely reported in the literature. The aim of this study was to provide a procedure for the mechanical characterization of urethral tissues and structures. The experimental protocol included the morphometric and histological analysis of urethral tissues, the mechanical characterization of the response of tissues to tensile and stress-relaxation tests and evaluation of the behaviour of urethral structures by inflation tests. Results from the preliminary experiments were processed, adopting specific model formulations, and also providing the definition of parameters that characterize the elastic and

DOI: 10.1113/EP085476

viscous behaviour of the tissues. Different experimental protocols, leading to a comprehensive set of experimental data, allow for a reciprocal assessment of reliability of the investigation approach.

(Received 7 August 2015; accepted after revision 4 February 2016; first published online 10 February 2016)
Corresponding author A. N. Natali: Department of Industrial Engineering, Centre for Mechanics of Biological Materials, University of Padova, Via F. Marzolo, 9, I-35131 Padova, Italy. Email: arturo.natali@unipd.it

Introduction

Lower urinary tract dysfunction is common in both men and women (Abrams *et al.* 2002), with the incidence increasing with age. Incontinence affects ∼400 million people worldwide (Hampel *et al.* 2004; Irwin *et al.* 2006), with a strong social and economic impact (Minassian *et al.* 2003). Different congenital or acquired pathologies determine the anatomical and functional alterations of the bladder–sphincter–urethra apparatus, with consequent debilitating incontinence (Nitti, 2001; Delancey & Shton-Miller, 2004). Lower urinary tract dysfunction may cause storage (51% of men and 59% of women), voiding (26% of men and 20% of women) and postmicturition symptoms (17% of men and 14% of women; Rosen *et al.* 2003; DuBeau, 2006; McVary, 2006; Thüroff *et al.* 2011). Patients with symptoms of lower urinary tract dysfunction experience a reduction in their quality of life (Van Kerrebroeck *et al.* 1993; Braun *et al.* 2003; McVary, 2006). Nowadays, surgical treatments and prosthetic devices are available, but their reliability and durability should be investigated further. Artificial urinary sphincter devices allow continence (Börgermann *et al.* 2010; Thüroff *et al.* 2011) by means of occlusion obtained by the application of a constant pressure (Chung, 2014). The mechanical action of the sphincter is usually also defined to ensure continence in the case of high-pressure conditions in the bladder (Hached *et al.* 2014; Singla *et al.* 2015). Consequent mechanical effects on the urethral tissues may induce some modifications (Baskin *et al.* 1993; Cavalcanti *et al.* 2007; Mundy & Andrich, 2011) and possible degenerative phenomena (Hajivassiliou & Finlay, 1999; Hampson *et al.* 2014; Bates *et al.* 2015). Moreover, the prosthetic device can have a limited durability (Fowler *et al.* 1993; Montague *et al.* 2001; Andreasson *et al.* 2014).

The design of an artificial urinary sphincter is mostly performed on a clinical and surgical basis, but it should be supported by investigation of its mechanical interaction with the surrounding tissues. In this way, it is possible to identify the sphincter pressure conditions that ensure continence, as well as the conformation of the device to minimize the invasiveness of the prosthesis (Chung, 2014; Hached *et al.* 2014; Ramesh *et al.* 2014). For this purpose, Marti *et al.* (2006) developed an empirical compression model based on the mechanical properties of the urethra, taking into account characterization of explanted animal or human urethras. They found that the occlusion pressure depends on the bladder pressure and the occlusion force is a linear function of the length of the artificial sphincter. In this work, several animals (including pigs, dogs, sheep and calves) were compared in order to find a suitable model for *ex vivo* characterization. Experimental investigation on humans is complex and must take into account an extended group of subjects of similar age, body conformation and health conditions. At present, experimental testing on human urethrae is performed *in vivo* (Griffiths, 1971*a*,*b*; Thind, 1995; Bagi *et al.* 2002; Comiter *et al.* 2003; Mijailovich *et al.* 2007; Ishii *et al.* 2014).

In order to carry out *ex vivo* tests, a suitable animal model should be selected (Fry *et al.* 2010), presenting similarity to the human penile urethra in terms of histology and overall conformation. Small rodents are not taken into consideration owing to the different size and structure of the lower urinary tract (Nozaki, 1959; Neuhaus *et al.* 2001; Maia *et al.* 2006). In mammals, the penis may present two main different conformations (König & Liebich, 2009) with regard to fibroelastic or musculocavernous components. Ruminants and swine have a fibroelastic penis, with small blood septa divided by a relevant amount of fibroelastic tissue and enclosed by a thick albuginea tunic surrounding both the cavernous and the spongy body (Babinski *et al.* 2005). In these animals, the penis exhibits a sigmoid flexure at the level of the thighs. Moreover, in small ruminants, a free urethral process prolongs the urethra beyond the glans (König & Liebich, 2009). Owing to the presence of the sigmoid flexure and urethral process, the structure of the penile urethra of these species may entail difficulties in experimental testing and comparison with humans. Nonetheless, swine urethra was demonstrated to show similarities to human urethra, concerning functionality and mechanical behaviour (Marti *et al.* 2006; Joller *et al.* 2012). Stallions and carnivores, in contrast, have a musculocavernous penis, with larger septa in the cavernous and spongy regions and a greater amount of muscle fibres (Budras *et al.* 2001), with an overall conformation that is comparable to the human penis, with some approximation. Between these last two groups, also considering the availability of samples, the horse was assumed to represent a suitable model for *ex vivo* characterization. In general, it should be remarked that a limit of any animal model is an uncertain correlation with

humans about changes in mechanical properties owing to age and health conditions.

The equine urethra can be considered similar to the human urethra in terms of the lumen, histomorphometric conformation (Dellmann & Eurell, 1998; Wolfe & Moll, 1999; Pozor & McDonnell, 2002; Barone, 2003; Arrighi *et al.* 2004) and functional process of micturition (Clark *et al.* 1987; Ronen, 1994; Brading, 1999). These reasons motivate the selection of horse urethra for investigation of the biomechanical response of the urethra under sphincteric contraction. For this purpose, computational methods can be adopted for the analysis of biological tissues and structural response, mostly with regard to the evaluation of the lumen occlusion process. The development of reliable computational models requires the exhaustive experimental characterization of the constituent tissues (Natali *et al.* 2009) through histological analysis and mechanical testing. The experimental results allow the definition of an appropriate constitutive formulation and identification of the related constitutive parameters. The histological analysis aims to identify the configuration of tissues, including the content of collagen or muscle fibres in the different layers. This information allows a preliminary hypothesis to be formed regarding the mechanical behaviour, and also suggesting the experimental tests to develop. Tubular organs, such as the urethra, can be characterized by investigating different specimen typologies. Different-shaped samples are harvested from the urethral wall, depending on the specific test loading condition. Tissue mechanical tests, together with information about the microstructural configuration of the tissue, allow the preliminary identification of the constitutive model and the related parameters (Gasser *et al.* 2006). Additional tests must be developed at the structural level, such as inflation tests on tubular segments, in order to evaluate the overall structural response (Hoeg *et al.* 2000; Gregersen, 2003; Carniel *et al.* 2014). Remarks in the literature pertaining to the evaluation of mechanical properties of animal and human urethra are limited (Abramowitch *et al.* 2009). *In vitro* and *in vivo* characterization of urethrae from animal models has been performed by different authors (Lecamwasam *et al.* 1999; Marti *et al.* 2006; Lalla *et al.* 2007; Feng *et al.* 2010; Haworth *et al.* 2011; Joller *et al.* 2012). However, these studies do not always discuss similarities with humans and do not take into account a combination of tissue and structural tests, without providing a throughout investigation. The present experimental protocol includes histological analysis, tensile and stress-relaxation tests of the urethral tissues and inflation tests of urethral structure.

Methods

Ethical approval

All experiments were conducted on tissues collected at a local abattoir and taken from carcasses of animals slaughtered normally, in compliance with the Italian and European laws (Council Directive 93/119/EC, Council Regulation no. 1099/2009, Law no. 131/2013). No live animal was killed for this research.

Sample collection and dissection

Fresh penises from 15 male saddle horses were obtained from a local slaughterhouse. The horses were 4–11 years old and 300–400 kg in weight. All the animals were intact and clinically healthy. Within 15 min from slaughter of the horse, the penis was harvested (Fig. 1*A*), packed in

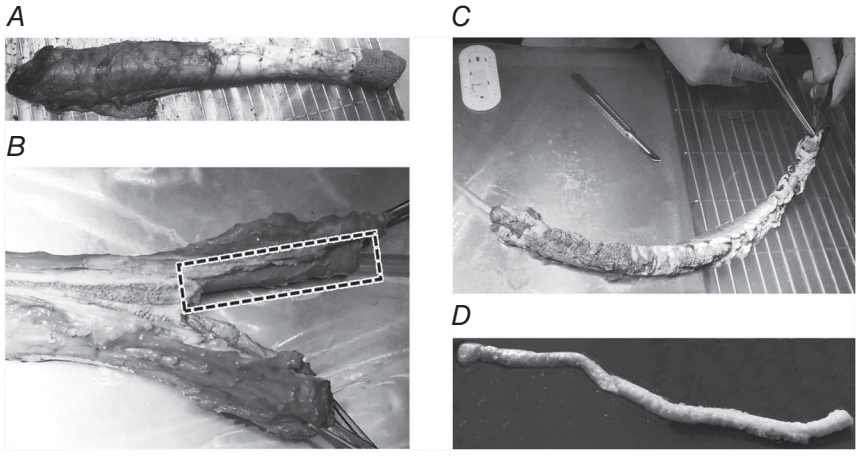

Figure 1. Procedure for dissection of the horse urethra
A, intact horse penis. *B*, cutting of the corpora cavernosa up to the albuginea; the dashed box indicates the urethra. *C* and *D*, dissected urethra before (*C*) and after (*D*) final cleaning from residuals of surrounding tissues.

physiological saline solution at 4°C and transported to the laboratory. The penises were carefully cleaned with cold physiological saline solution to eliminate skin debris. Next, glands and the skin were surgically removed. A soft urinary catheter was temporarilyy inserted in the lumen of the urethra to serve as a palpable guide for facilitating the correct identification of the shape. A surgical incision was performed on the lateral aspect of the penis, between the tunica albuginea and the bulbospongiosus muscle (Fig. 1*B*). By blunt dissection, the corpus cavernosum was separated from the bulbospongiosus muscle surrounding the urethra, starting from the proximal part of the penis. The dissection continued from the proximal end of the penis to the distal end, isolating the penile urethra (Fig. 1*C*). During dissection, the sample was continuously dampened with cold physiological saline solution to preserve the tissues. The dissected urethra was cleaned from bulbospongiosus muscle and residual surrounding tissues. Finally, the urethral sample was composed of the lumen surrounded by the corpus spongiosum (Fig. 1*D*). The length of the urethra was about 400–450 mm.

Two urethrae were assigned to histological investigation, stored in formaldehyde for fixation. The other 13 urethrae were divided to provide the specimens for the mechanical tests of urethral tissues and structures. The most proximal and the most distal regions of each urethra were assigned to tensile and stress-relaxation tests. The residual parts of the urethrae were almost equally divided into two segments to provide proximal and distal specimens for inflation tests. All the mechanical tests were concluded within 6 h from the slaughter of the animal, at room temperature. Previous experiences confirm that similar temperature conditions do not alter the mechanical response of soft tissues (Van Mastrigt & Nagtegaal, 1981; Salinas *et al.* 1992; Nagatomi *et al.* 2004).

Histological analysis

The straightened urethrae were stored in 10% neutral buffered formalin. Fixation was performed at room temperature for ∼72 h. After fixation, urethral samples with a thickness of 3 mm were cut every 50 mm in a transverse direction. Each sample was then stored in a histological cassette and processed to replace formalin with paraffin. Tissue processing was performed using a Shandon Excelsior Tissue Processor (Thermo Fisher Scientific Inc., Waltham, MA, USA). Samples were subsequently dipped into different alcohol solutions (50, 70 and 90%), absolute ethanol and xylene, and three paraffin baths for 90 min each. Finally, paraffin wax at 60°C was poured into the cassette to cover the sample entirely. The cassette was cooled for 24 h at −20°C before microtomy. A Leica RM2145 microtome (Leica Microsystems Srl, Milano, Italy) was set to cut 4-μm-thick sections. By means of serial sectioning, ∼250 transverse sections were obtained from each sample. Among these, five equally spaced sections were selected for quantitative identification of morphological properties and the amount of collagen and muscular fibres. Longitudinal sections were prepared using a similar procedure, by dissecting one sample for each urethra in the most proximal region.

Histological sections were placed in water and selected using a glass slide. The slides were stationed to dry the section and to dissolve the paraffin wax. A few sections were stained with Haematoxylin and Eosin for a preliminary evaluation of the tissue conformation, whereas Masson trichrome staining with Aniline Blue was performed on the other sections to emphasize the different components of the urethral tissues, such as collagen, muscle fibres and cells (Bancroft & Gamble, 2008). The slides were first examined using an optical Leica DMD 108 microscope (Leica Microsystems Srl) for qualitative identification of the tissue conformation. Finally, digital pictures of the urethral sections were analysed using the image-processing toolbox Matlab (The MathWorks Inc., Natick, MA, USA) to quantify geometrical properties and the percentage of collagen and muscle fibres.

Mechanical tests of urethral tissues

Mechanical tests of urethral tissues were performed on specimens from both distal and proximal regions. Each segment was cut longitudinally (Fig. 2*A*) and straightened on a metal plate (Fig. 2*B*). Rectangular specimens (with a grip-to-grip length of ∼20 mm and width ∼5 mm) were dissected along longitudinal and circumferential directions (Fig. 2*C*). Depending on the specific segment size, two to four specimens for each cutting direction were prepared. Digital image processing was used to measure sample thickness and width at different positions. Cross-sectional area of each specimen was calculated assuming mean values of thickness and width. The samples were continuously dampened with physiological saline solution at room temperature during the preparation and testing. The number, grip-to-grip length, width and thickness of the specimens are reported in Table 1.

A Bose ElectroForce machine (Bose Corp., ElectroForce Systems Group, Eden Prairie, MN, USA) was used to perform tensile tests. Each specimen was stretched up to 60% strain, and the strain was then kept constant for 300 s to investigate stress-relaxation phenomena. Based on a preliminary evaluation of the tissue stiffness, a load cell with capacity of 20 N with accuracy of ±0.1% was

adopted. Preliminary tests were also performed to evaluate the influence of strain rate on viscous effects. The results showed that a 60% s^{-1} strain rate minimizes the influence of viscous phenomena (Thind, 1995; Bagi *et al.* 2002) and prevents the dynamic effects that may develop when higher strain rates are adopted (Fung, 1993; Weiss & Gardiner, 2001). In order to hold the specimen at its ends, two patches of balsa wood were glued to each end of the sample (Fig. 2*D* and *E*) and interposed between the grips. The pressure of the grips was adjusted to avoid slippage and damage of the specimens. The strain was computed as the ratio between the elongation and the initial grip-to-grip length. The stress was calculated as the ratio between force measured by the load cell and the initial cross-sectional area of the specimen. Data from stress-relaxation tests were processed to identify the reduction of normalized stress with time. The normalized stress is defined as the ratio of the stress at the present time and the peak stress at the beginning of the relaxation phase.

The median curves and the related 50% probability scatter bands are reported in terms of stress–strain and normalized stress–time. These curves were calculated separately for distal or proximal and longitudinal or circumferential specimens. Exponential functions were adopted to interpret stress–strain and stress–time behaviour and to obtain preliminary information about elastic and viscous behaviour of the tissue, as follows:

$$\sigma(\varepsilon) = \frac{k}{\alpha}[\exp(\alpha\varepsilon) - 1] \quad (1)$$

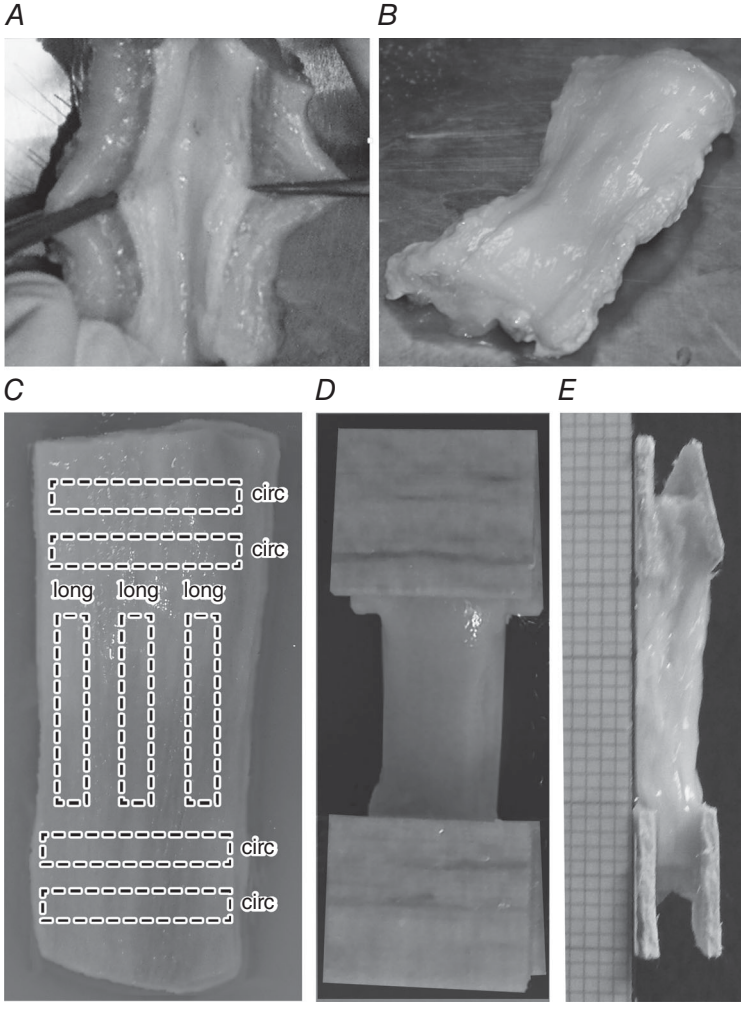

Figure 2. Preparation of samples for mechanical tests of urethral tissues
A and *B*, the tubular segment is cut longitudinally (*A*) and straightened (*B*). *C*, tissue specimens are dissected according to a rectangular shape; two to four specimens are prepared along longitudinal and circumferential directions. *D* and *E*, patches of balsa wood are glued to the sample ends to enable the specimen to be gripped; frontal (*D*) and lateral views (*E*).

Table 1. Geometrical conformation of tissue samples for mechanical tests of the urethral tissues

Region and direction	No. of tissue samples	Grip-to-grip length (mm)	Width (mm)	Thickness (mm)
Proximal region, circumferential direction	34	18.23 (17.14, 21.53)	4.98 (4.58, 5.36)	2.49 (2.36, 3.34)
Proximal region, longitudinal direction	33	20.36 (18.57, 22.28)	5.52 (4.87, 6.98)	3.21 (2.56, 3.56)
Distal region, circumferential direction	36	20.45 (14.38, 20.12)	6.18 (4.79, 9.20)	4.06 (3.19, 5.72)
Distal region, longitudinal direction	32	20.18 (18.67, 21.03)	7.47 (5.72, 8.35)	3.89 (2.86, 5.05)

Median values (25th, 75th percentiles) are reported.

$$\sigma^{\mathrm{norm}}(t) = (1-\gamma_1-\gamma_2) + \gamma_1 \exp\left(-\frac{t}{\tau_1}\right) + \gamma_2 \exp\left(-\frac{t}{\tau_2}\right) \quad (2)$$

Equation (1) aims at interpreting the non-linear stress (σ) *versus* strain (ε) response of the tissue during loading. The parameter k specifies the tissue initial stiffness, while α is related to the non-linearity of the response due to stiffening. Equation (2) interprets the exponential decay of the normalized stress σ^{norm} with time t because of stress-relaxation phenomena. Equation (2) accounts for two viscous branches. The number of viscous branches was defined contemporaneously to minimize the number of parameters and correctly interpret the trend of experimental data. According to the standard theory of viscoelasticity (Holzapfel, 2000), the parameter $\gamma_\infty = 1-\gamma_1-\gamma_2$ identifies the ratio between the equilibrium stress (when relaxation phenomena are completed) and the peak stress (at the beginning of the relaxation phase). The parameters τ_1 and τ_2 are the time constants of relaxation. Data from tensile and stress-relaxation tests developed on each specimen were fitted by eqns (1) and (2), respectively. The minimization of the discrepancy between experimental data and model results represents a non-linear least-squares problem, solved by using the 'lsqnonlin' function in Matlab and adopting the trust region reflective algorithm to minimize the residual sum of squares (RSS). The RSS is defined as follows:

$$\mathrm{RSS} = \sum_{i=1}^{n} \left(f_{\mathrm{exp},i} - f_{\mathrm{num},i}\right)^2$$

where n is the total number of experimental data, $f_{\mathrm{exp},i}$ is the ith experimental datum and $f_{\mathrm{num},i}$ the corresponding ith model result. Statistical data of the elastic parameters k and α and of the viscous parameters γ_1, γ_2, τ_1 and τ_2 were computed, allowing a preliminary evaluation of the influence of specimen location and direction on tissue mechanical properties.

The effects of the imposed strain on the results from tensile tests were evaluated by means of a multivariate ANOVA, considering three levels of strain (10, 20 and 40%) and comparing the mean stress values among different groups of samples (proximal longitudinal, proximal circumferential, distal longitudinal and distal circumferential samples). The same kind of analysis was performed for the statistical interpretation of results from stress relaxation by evaluating the stress-relaxation process at four time instants (1, 10, 100 and 300 s) and by making a comparison of the mean stress value of each of the above-mentioned groups with the others.

Mechanical tests of urethral structure

Mechanical tests of urethral structure were performed on tubular specimens taken from distal and proximal regions. Each sample was placed over a metal plate and straightened along the longitudinal direction. Two small slices of the sample (~3 mm in length) were removed at the extremities. The length of the remaining tubular portion was measured with digital callipers. The extremity slices were used to measure the urethral wall thickness and external diameter. The number and morphological characteristics of the samples concerning length, external diameter and wall thickness are reported in Table 2.

The proximal extremity of the sample was fixed by means of a surgical elastic seam to a Teflon cannula with internal and external diameters of 4 and 6 mm, respectively. The other extremity was sealed to prevent any liquid leak (Fig. 3*A*). The sample was placed over a Teflon plate and straightened along the longitudinal direction. The cannula was also connected to a mechano-electrical transducer (142 pc 01d pressure transducer; Honeywell, USA) that was interfaced to a data storage device (1326 Econo Recorder; BioRad, Italy).

The inflation test was performed according to a two-step procedure. The first step was an almost instantaneous liquid inflow, up to a prescribed volume of inflation (Fig. 3*B*). Therefore, in this phase an elastic response of the structure may be assumed. In the second step, the volume of the sample was held constant for ~300 s to allow the development of viscoelastic processes, up to steady-state conditions. Five to seven inflation tests were performed on each sample according to different inflation volumes, ranging between 5 and 50 ml. The inflation time was always <0.1 s. During the test, physiological

Table 2. Geometrical conformation of tubular samples for mechanical tests at the structure level

Region	No. of tissue samples	Seam-to-seam length (mm)	Internal diameter, proximal (mm)	Internal diameter, distal (mm)	External diameter, proximal (mm)	External diameter, distal (mm)	Internal volume (mm^3)
Proximal region	12	71.24 (55.32, 80.27)	7.13 (6.21, 8.36)	6.08 (4.72, 7.03)	15.37 (14.28, 18.19)	13.16 (12.42, 14.31)	2.90 (2.60, 5.89)
Distal region	11	65.38 (57.16, 98.22)	5.03 (4.79, 6.27)	4.06 (3.96, 4.21)	13.25 (12.83, 14.27)	11.08 (9.76, 13.18)	2.45 (2.02, 2.54)

Median values (25th, 75th percentiles) are reported.

saline solution was poured onto the external surface of the samples to prevent drying.

To compare samples with morphological differences, the volume data were homogenized by considering the ratio between sample volume during testing and sample volume at rest $v = \Delta V/V_0$, where v is the volumetric ratio, ΔV the inflated volume and V_0 the initial volume of the sample. The initial volume, V_0, was obtained from the shape of the sample during experimental testing. Median curves of pressure *versus* volumetric ratio and normalized pressure *versus* time, with the associated 50% probability scatter bands, were computed for inflation and relaxation tests on proximal and distal samples. The normalized pressure was obtained as the ratio of the pressure at present time and the peak pressure at the beginning of the relaxation phase.

Exponential functions were adopted to interpret the behaviour of pressure *versus* volumetric ratio and normalized pressure *versus* time to identify preliminary information about the structural elastic and viscous response of the tubular structure (Carniel *et al.* 2014), as follows:

$$P(v) = \frac{K}{A}[\exp(Av) - 1] \quad (3)$$

$$P^{\text{norm}}(t) = (1 - \Gamma_1 - \Gamma_2) + \Gamma_1 \exp\left(-\frac{t}{T_1}\right) + \Gamma_2 \exp\left(-\frac{t}{T_2}\right) \quad (4)$$

Equation (3) describes the pressure (P) *versus* volumetric ratio (v) response of the tissue during the inflation step. The parameter K specifies the initial stiffness of the tubular segment, while A is related to the non-linearity of the mechanical response because of stiffening phenomena. Equation (4) describes the exponential decay of normalized pressure P^{norm} over time t because of viscoelastic phenomena. The parameter $\Gamma_\infty = 1 - \Gamma_1 - \Gamma_2$ identifies the ratio between the pressure when viscoelastic phenomena are completed and the peak pressure at the beginning, while T_1 and T_2 are parameters related to structural relaxation times. Data from tests developed on each specimen were fitted by eqns (3) and (4), respectively. The fitting of the models to experimental data is obtained with the same procedure adopted for tissue samples. Also, in this case, statistical data of the elastic parameters K, A and of the viscous parameters Γ_1, Γ_2, T_1 and T_2 were computed.

The multivariate ANOVA was applied to data from inflation and relaxation tests with the same method described above, distinguishing samples into two groups (proximal and distal).

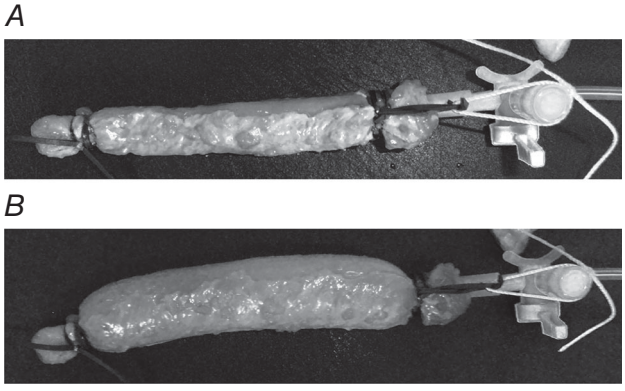

Figure 3. Preparation of samples and mechanical testing at the structure level
The proximal end of the tubular sample is fixed by means of a surgical elastic seam to a Teflon cannula, attached to a syringe, whereas the other end is hermetically sealed. *A* and *B*, not inflated (*A*) and inflated conformations (*B*) of a typical experimental sample.

Results

Histological analysis

The analysis of histological samples allowed evaluation of the structural components of the urethra and their distribution. Figure 4 shows a histological view of a transverse section of the most proximal urethra. The trichrome staining makes it possible to identify the

tissue conformation and the components (Fig. 4*A*). A mucosal layer, surrounding the lumen of the urethra and the epithelium, was clearly identified as transitional epithelium (Fig. 4*B*). Above the mucosa, there is a layer of dense connective tissue showing an arrangement of collagen fibrils (Fig. 4*C*). Above the dense connective tissue, there was a loose tissue containing the corpora spongiosa, blood vessels and smooth muscle fibres (Fig. 4*A*). The observation of muscular structures on subsequent transverse serial sections suggested the preferential alignment of muscle fibres along the urethra in a longitudinal direction. The orientation of muscular structures was confirmed by the histological analysis of longitudinal sections (Fig. 5). The amount of smooth muscle fibres was very much larger in the proximal region of the urethra than in the distal portion (Fig. 6). Image processing allowed quantitative identification of the muscle and collagen fibre content, which showed a linear decreasing and increasing trend, respectively, when moving from the proximal to the distal region of the urethra. A linear correlation between the percentage and position of each component ($r^2 > 0.8$) was found both for muscle (Fig. 6*A*) and connective fibres (Fig. 6*B*). The urethra section area (Fig. 6*C*) and lumen perimeter (Fig. 6*D*) showed a linear correlation with position ($r^2 > 0.7$). On the contrary, the lumen area varied around the median value of 5.14 mm^2, being 3.61 and 5.71 mm^2 at the 25th and the 75th percentiles, respectively.

Mechanical tests of urethral tissues

Generally, the results of mechanical testing showed that urethral tissue has a non-linear stiffening and time-dependent behaviour, which is also anisotropic only in the proximal region. The statistical distributions of the experimental results are shown in the graphs of Fig. 7, where median curves are reported together with the 50% probability scatter bands. Processing of the experimental curves from mechanical tests performed on the different

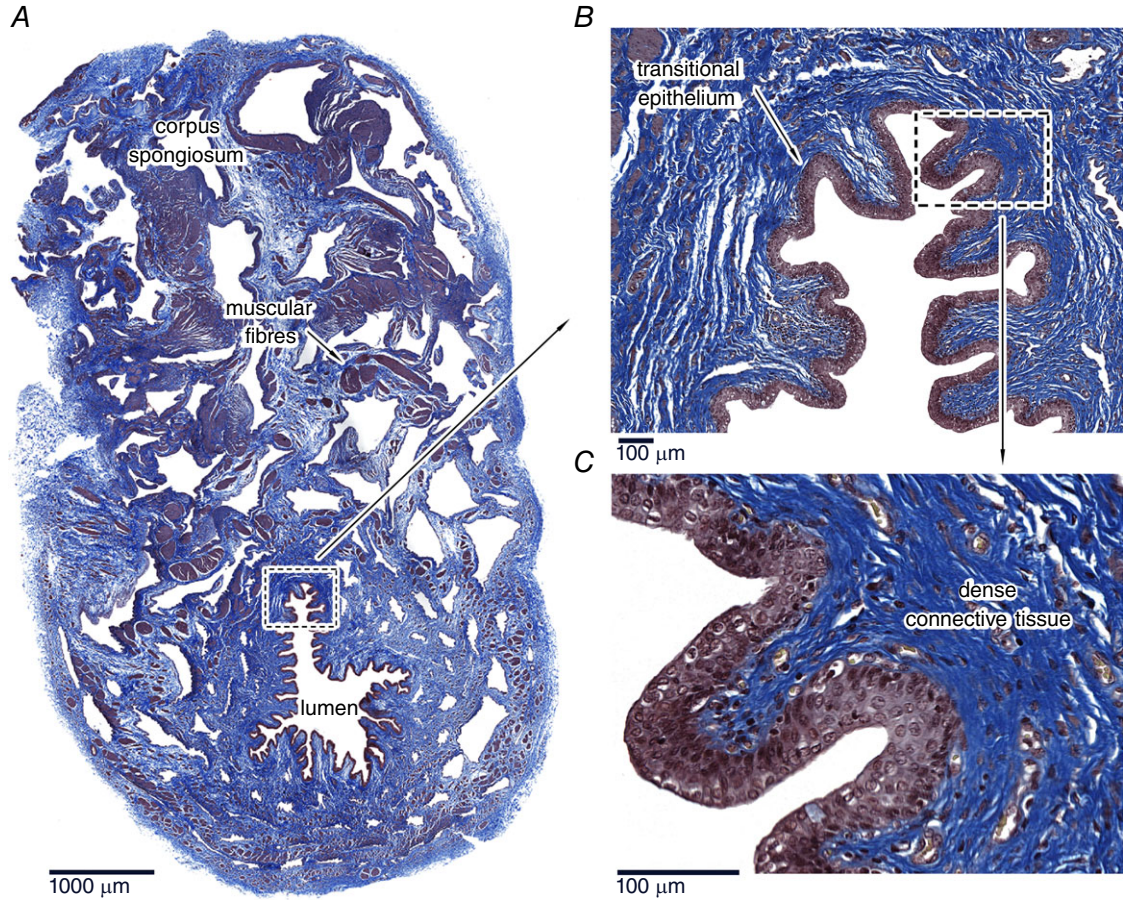

Figure 4. Trichrome histological section of the proximal urethra
General view of a transverse section of the urethra (*A*) and details (*B* and *C*) to show the conformation of the epithelium and connective tissues surrounding the lumen. The section was obtained 50 mm from the most proximal end of the urethra.

samples led to a preliminary evaluation of elastic and viscous parameters, whose statistical distributions are reported in Table 3. The analysis of median curves made it possible to identify further sets of parameters (Table 4). Such parameters should interpret the general trend of the experimental data.

Mechanical tests of urethral structure

Experimental results on the urethral structure are reported in Fig. 8 by means of median curves and 50% probability scatter bands. Also in this case, a non-linear stiffening is evident during inflation and time-dependent phenomena in the following step. Distributions of structural parameters were achieved by processing experimental data from the different samples (Table 5) and median curves (Table 6).

Discussion

Owing to the lack of thorough knowledge of urethral tissues and structures, this preliminary investigation was carried out with the aim of defining an experimental protocol to investigate the mechanical behaviour of the urethra. The proposed experimental activities were developed on horse urethra, because of the similar configuration of equine and human tissues (Cavalcanti *et al.* 2007; Wu *et al.* 2010; Tziannaros *et al.* 2013) and the ready availability of *ex vivo* samples. The analysis accounted for the identification of the macro- and microstructural configuration of the tissues through morphological and histological analysis. The mechanical behaviour was investigated by means of experimental tests of the urethral tissues (tensile and stress-relaxation tests) and structure (inflation tests).

Regarding the morphology, in both human and equine penis, a transitional epithelium and a thin layer of dense connective tissue surround the lumen. Outside these layers, the urethra is composed of loose tissue containing the corpora spongiosa, blood vessels and smooth muscle fibres. Histological analysis of horse urethra showed different micro- and macrostructural conformations of the urethral section when moving from the proximal to the distal region (Fig. 6). The area of the section progressively decreased (Fig. 6*C*). The area of the occluded lumen did not change significantly, whereas the lumen perimeter progressively increased (Fig. 6*D*). The amount of collagen fibres was relevant along the whole urethra, with a marginal decrease in the proximal region (Fig. 6*B*). The amount of muscle fibres decreased from the proximal to the distal urethra (Fig. 6*A*). Muscle fibres were preferentially oriented along the longitudinal direction. In the thin layer of dense connective tissue around the lumen, collagen was arranged along the lumen perimeter (Fig. 6*C*).

Tensile tests on specimens from the proximal region showed greater stiffness along the longitudinal direction than along the circumferential direction (Fig. 7*A*). This fact was supported by the multivariate ANOVA at different strain levels (10, 20 and 40%), which highlighted a significant difference ($P < 0.001$) between the longitudinal proximal samples and all the other samples (circumferential proximal, longitudinal distal and circumferential distal). The spatial orientation of muscle fibres along the longitudinal direction can explain the anisotropic behaviour in the proximal region.

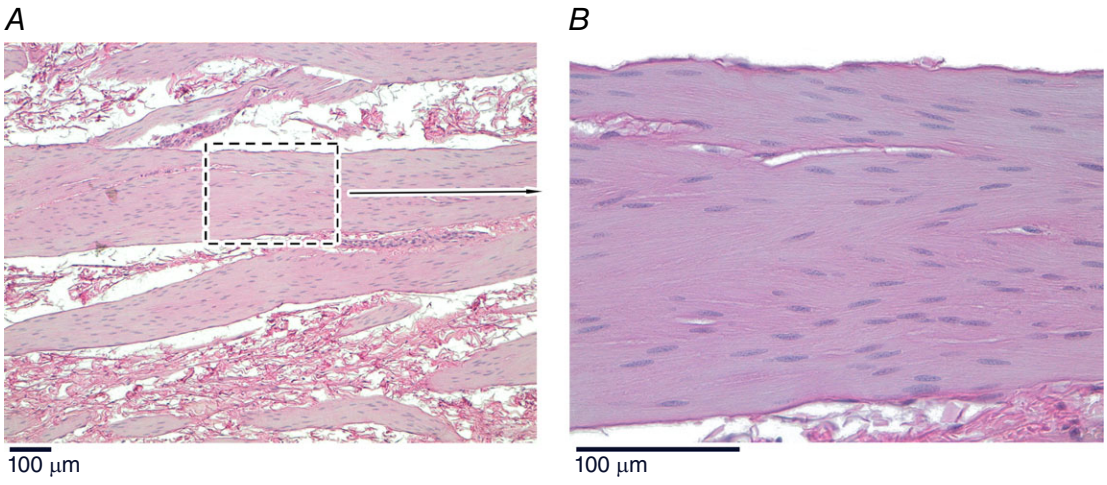

Figure 5. Histological section of the proximal urethra
A, general view of muscle structures in a longitudinal section. *B*, detail to highlight the inner conformation of muscle components.

On the contrary, the multivariate ANOVA showed no significant differences ($P > 0.05$) between longitudinal and circumferential specimens from the distal region (Fig. 7*C*). Furthermore, no significant differences ($P > 0.05$) were found between all distal specimens and circumferential specimens from the proximal region.

Regarding the stress-relaxation tests, the viscoelastic behaviour showed little dissimilarity among the considered groups of samples (longitudinal proximal, circumferential proximal, longitudinal distal and circumferential distal; Fig. 7*B* and *D*). Indeed, the multivariate ANOVA considering data from stress relaxation at different times (1, 10, 100 and 300 s) did not highlight statistically significant differences among the above-mentioned groups ($P > 0.05$).

Data from mechanical tests of the urethral structure showed a larger structural stiffness (Fig. 8*A*) and a higher percentage of pressure relaxation for the proximal urethra when compared with the distal urethra (Fig. 8*B*). These differences were confirmed by the multivariate ANOVA performed on instantaneous inflation ($P < 0.001$) and pressure-relaxation data ($P < 0.01$), respectively, at the

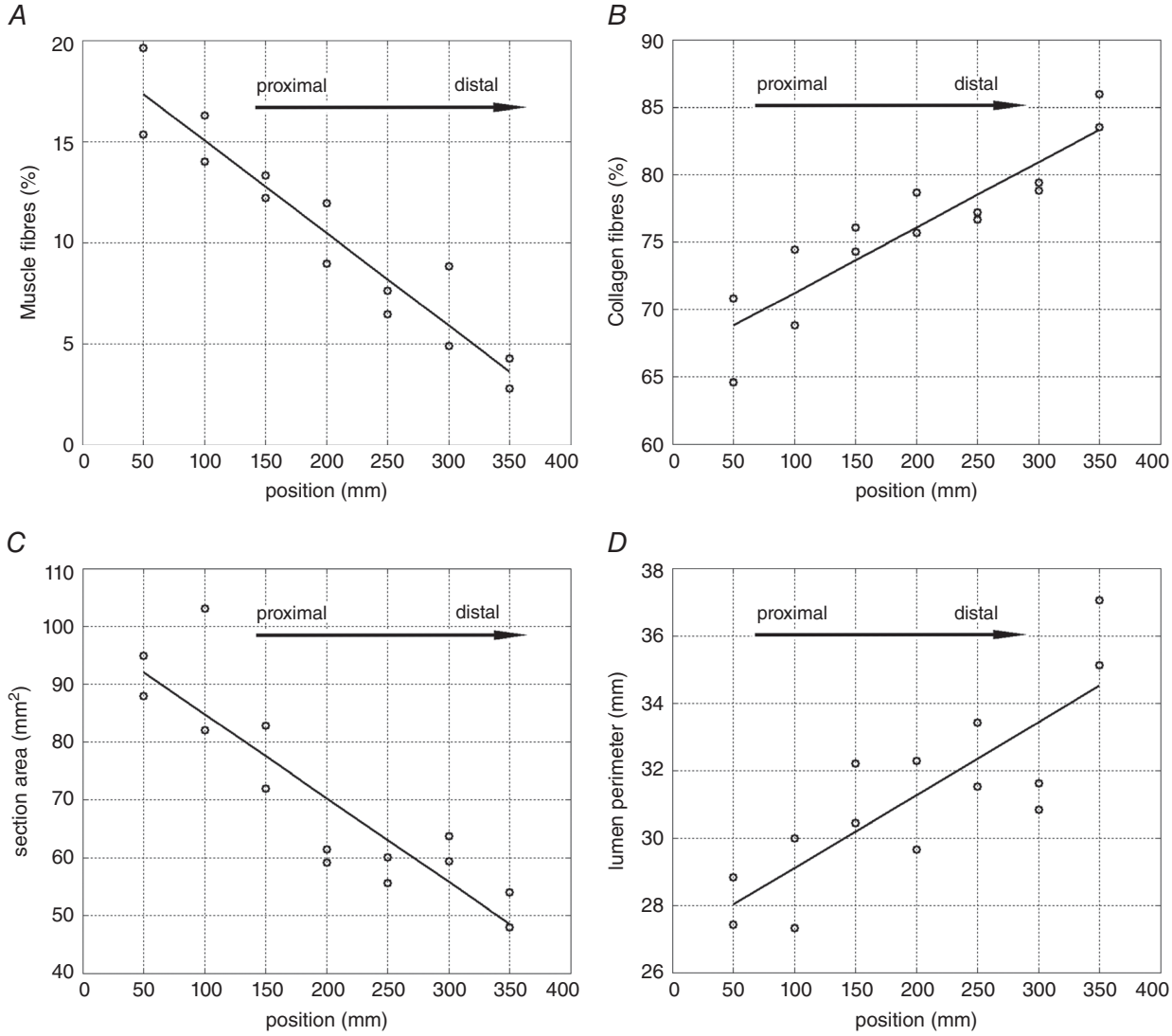

Figure 6. Quantitative analysis of histology of the urethra
Postprocessing of histological images shows the almost linear correlation between muscle content (*A*) or collagen content (*B*) and positioning. In addition, geometrical properties, such as the urethra section area (*C*) and the lumen perimeter (*D*), show good linear correlation with position. The experimental data at 50 mm from the most proximal end correspond to the histological section shown in Fig. 5. Measurement errors are ±5% of experimental values for muscle, collagen fibres and section area, ±0.5 mm for lumen perimeter and ±0.1 mm for position.

same percentages and times of the analyses on tissue samples.

The number of urethral samples is considered reasonably high for the present study. However, the investigation of a larger number of samples would enable statistical analysis and experimental data reliability to be improved.

The results of the mechanical tests can be related to the microstructure of the urethral tissue evidenced by histological analysis. With particular regard to the proximal region of the urethra, the histology showed a preferential orientation of muscle fibres along the longitudinal direction that may be regarded as the reason for tissue anisotropy. Moreover, the amount of muscle fibres was found to decrease from the proximal to the distal urethra. Owing to this conformation, tissue stiffness is higher in the proximal region and along the longitudinal direction. This method leads to a qualitative correlation, which could be supported by quantitative measurements on the mechanical properties of collagen fibres, based on additional histological and mechanical characterization. Moreover, the three-dimensional microstructure of the urethra could be investigated in detail by microcomputed tomography in absorption and phase contrast modes (Müller *et al.* 2010).

Structural rearrangement processes produce stress-reduction phenomena influencing the amplitude and duration of viscoelastic phenomena, which are quantitatively

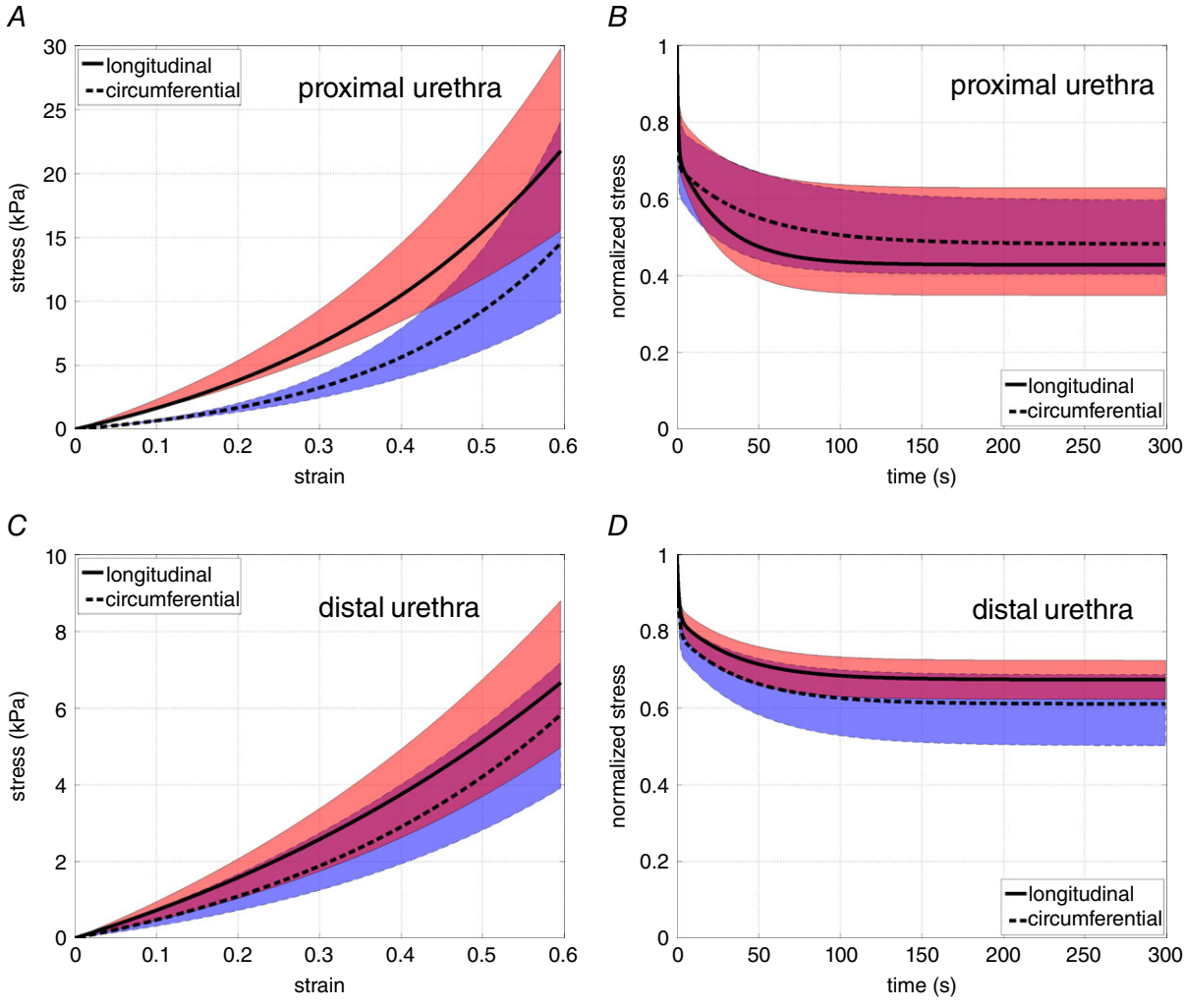

Figure 7. Results from mechanical tests of the urethral tissues
Tests were performed on specimens from proximal (*A* and *B*) and distal regions (*C* and *D*) of the urethra and accounting for constant strain rate (*A* and *C*) and stress-relaxation conditions (*B* and *D*). Median curves are reported together with 50% probability scatter bands. Data pertain to tests performed along both longitudinal (continuous lines and pink bands) and circumferential directions (dashed lines and blue bands). Violet regions indicate the superposition of longitudinal and circumferential scatter bands.

Table 3. Identification of tissue parameters by analysis of mechanical tests of the urethral tissues: statistical distribution of elastic and viscous parameters

Region and direction	k (kPa)	α	γ_1	γ_2	τ_1 (s)	τ_2 (s)
Proximal region, circumferential direction	4.88 (4.55, 8.95)	3.48 (2.98, 4.97)	0.33 (0.24, 0.43)	0.17 (0.15, 0.18)	0.87 (0.73, 1.78)	51.66 (48.14, 62.67)
Proximal region, longitudinal direction	15.66 (13.59, 18.89)	2.11 (1.62, 2.75)	0.33 (0.21, 0.37)	0.24 (0.15, 0.28)	1.40 (1.03, 1.77)	38.92 (35.97, 42.11)
Distal region, circumferential direction	3.84 (2.61, 8.93)	2.30 (1.83, 2.67)	0.24 (0.19, 0.29)	0.16 (0.13, 0.22)	1.98 (1.45, 2.68)	59.09 (51.00, 64.41)
Distal region, longitudinal direction	6.35 (3.86, 8.33)	1.63 (1.44, 1.83)	0.18 (0.16, 0.20)	0.15 (0.10, 0.15)	1.84 (1.51, 1.95)	47.47 (40.39, 48.37)

Median values (25th, 75th percentiles) are reported. k is the initial stiffness, α is a constant related to the non-linearity due to stiffening, γ_1 and γ_2 are relative stiffness parameters, τ_1 and τ_2 are the time constants of relaxation.

Table 4. Identification of tissue parameters by analysis of mechanical tests of the urethral tissues: elastic and viscous parameters from median curves

Region and direction	k (kPa)	α	γ_1	γ_2	τ_1 (s)	τ_2 (s)
Proximal region, circumferential direction	5.41	4.22	0.33	0.18	0.74	52.72
Proximal region, longitudinal direction	14.41	2.75	0.32	0.26	1.07	37.02
Distal region, circumferential direction	4.46	2.32	0.23	0.17	1.46	51.13
Distal region, longitudinal direction	6.55	1.69	0.18	0.15	1.53	41.33

k is the initial stiffness, α is a constant related to the non linearity due to stiffening, γ_1 and γ_2 are relative stiffness parameters, τ_1 and τ_2 are the time constants of relaxation.

defined by the parameters γ_i, Γ_i, τ_i and T_i, respectively. The parameters γ_i and τ_i are computed by processing results from tests of the urethral tissues (Tables 3 and 4), whereas the parameters Γ_i and T_i account for data from tests of the urethral structure (Tables 5 and 6). Although the same microstructural rearrangement processes should be expected at tissue and structure levels, differences have been found between parameters. The differences

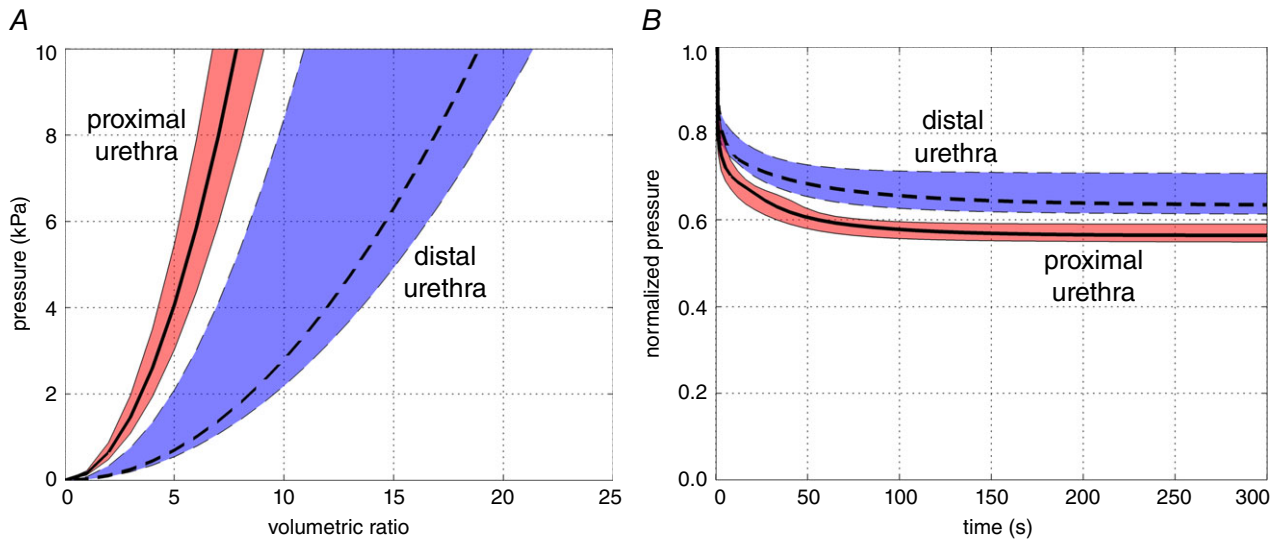

Figure 8. Results from mechanical tests performed at the structure level
Tests were performed on tubular specimens accounting for inflation (*A*) and stress-reduction conditions (*B*). Median curves are reported together with 50% probability scatter bands. Data pertain to tests performed on samples from proximal (continuous lines and pink bands) and distal regions (dashed lines and blue bands) of the urethra.

Table 5. Identification of structural parameters by analysis of mechanical tests at structure level: statistical distribution of structural elastic and viscous parameters

Region	K (kPa)	A	Γ_1	Γ_2	T_1 (s)	T_2 (s)
Proximal region	1.93 (1.38, 2.48)	0.19 (0.17, 0.20)	0.24 (0.20, 0.25)	0.20 (0.18, 0.24)	0.43 (0.39, 0.93)	23.85 (22.13, 28.16)
Distal region	0.32 (0.25, 0.95)	0.18 (0.16, 0.21)	0.18 (0.17, 0.19)	0.17 (0.15, 0.18)	0.74 (0.42, 0.78)	28.93 (26.88, 32.03)

Median values (25th, 75th percentiles) are reported. K is the initial stiffness, A is a constant related to the non-linearity due to stiffening, Γ_1 and Γ_2 are relative stiffness parameters, T_1 and T_2 are the time constants of relaxation.

Table 6. Identification of structural parameters by analysis of mechanical tests at structure level: structural elastic and viscous parameters from median curves

Region	K (kPa)	A	Γ_1	Γ_2	T_1 (s)	T_2 (s)
Proximal region	1.92	0.18	0.25	0.18	0.42	24.05
Distal region	0.33	0.18	0.20	0.16	0.72	29.94

K is the initial stiffness, A is a constant related to the non-linearity due to stiffening, Γ_1 and Γ_2 are relative stiffness parameters, T_1 and T_2 are the time constants of relaxation.

can be explained in part because the sample preparation for tissue tests requires dissection of the tubular urethra into rectangular specimens. The procedure may disrupt tissue continuity, with particular regard to collagen and muscle fibres, also modifying their rearrangement over time and viscoelastic phenomena. Probably for the same reason, the statistical analyses give different results when considering stress-relaxation tests and pressure-relaxation tests (proximal *versus* distal response).

The choice of the optimal number of viscous branches is based on the evaluation of the RSS for different numbers of viscous branches assumed. For experimental data on the relaxation of tissue samples, the fitting with two viscous branches gives an RSS value of the order of 10^{-2}. Concerning the inflation results, the fitting with two viscous branches makes it possible to find a lower RSS value, of the order of 10^{-3}. Therefore, the choice of two viscous branches for the models is suitable for describing the viscoelastic response of tissue and structures. The choice of an additional branch would enable a further reduction of the RSS value, resulting in a more complex model without effective improvement in the numerical simulation of the viscoelastic response.

The biomechanical properties of the urethral tissues of different animal models have been described in the literature. For example, inflation tests were carried out on urethral segments from female rats at distal and proximal locations to assess possible mechanical alterations resulting from vaginal pathologies (Prantil *et al.* 2007). In another study, the relaxation behaviour of pig urethra was monitored after inflation with different volumes of water (Idzenga *et al.* 2006). Despite the similarity in test procedures, the results of these studies are not comparable with the present work, because of the huge differences in the chosen animal model, sex, anatomy and tissue conformation (König & Liebich, 2009).

Aiming at the mechanical characterization of human urethra, the next step of the investigation will account for experimental activities on human samples. The evaluation of viscoelastic properties is extremely important for the description of the mechanical behaviour of urethral tissues and structure. At present, in computational modelling for urinary incontinence research, urethral tissues have frequently been simplified as linear elastic materials (Spirka *et al.* 2013; Brandão *et al.* 2015; Peng *et al.* 2015*a*). Instead, the viscoelastic properties of the urethral tissues should be taken into account. For this purpose, the mechanical tests proposed in the present work are the basis for the development of suitable viscoelastic constitutive models.

Moreover, uniaxial testing does not represent all loading conditions *in vivo*. For a more accurate mechanical evaluation, including an enhanced characterization of tissue anisotropy, biaxial tensile testing would be preferable, with loading being applied to a sample along two perpendicular axes, preferably corresponding to longitudinal and circumferential directions.

The compression behaviour of the urethra is also an aspect worth investigating. Further work is in progress to elucidate the mechanical response when sphincteric actions are applied, in order to evaluate the pressure conditions that may ensure continence, as proposed by Marti *et al.* (2006).

A complete biomechanical characterization of urethral tissues and structures *in vivo* cannot be achieved by using experimental techniques only. Computational models are suitable for providing additional information, on the basis of constitutive formulation and structural model

variations. For this purpose, numerical models of both equine and human urethra will be developed, accounting for the conformation of the different biological structures. This approach will make it possible to evaluate healthy and pathological conditions, providing new insights on lower urinary tract dysfunction and the performance of artificial urinary sphincters, slings (Peng *et al.* 2015*b*) or other prosthetic devices for urological surgery (Todros *et al.* 2015).

References

Abramowitch SD, Feola A, Jallah Z & Moalli PA (2009). Tissue mechanics, animal models, and pelvic organ prolapse: a review. *Eur J Obstet Gynecol Reprod Biol* **144**, S146–S158.

Abrams P, Cardozo L, Fall M, Griffiths D, Rosier P, Ulmstern U, van Kerrebroeck P, Victor A & Wein A (2002). The standardisation of terminology of lower urinary tract function: report from the Standardisation Sub-committee of the International Continence Society. *Neurourol Urodynam* **21**, 167–178.

Andreasson A, Fall M, Persson E, Stranne J & Peeker R (2014). High revision rate following artificial urethral sphincter implantation. *Scand J Urol* **48**, 544–548.

Arrighi S, Cremonesi F, Bosi G & Domeneghini C (2004). Endocrine-paracrine cells of the male urogenital apparatus: a comparative histochemical and immunohistochemical study in some domestic ungulates. *Anat Histol Embryol* **33**, 225–232.

Babinski MA, deBrito-Gitirana L, Chagas MA, Abidú-Figueiredo M, Costa WS & Sampaio FJB (2005). Immunohistochemical analysis of smooth muscle cells and volumetric density of the elastic system fibers of wild boar (*Sus scrofa*) penis. *Anim Reprod Sci* **86**, 317–328.

Bagi P, Bøtker-Rasmussen I & Kristensen J (2002). Pressure/cross-sectional area relations in the proximal urethra of healthy males: the time dependent pressure response following forced dilation. *Urol Res* **30**, 9–14.

Bancroft JD & Gamble M (2008). *Theory and Practice of Histological Techniques*, 6th edn. Elsevier, Churchill Livingstone, London, UK.

Barone R (2003). *Trattato di anatomia comparata dei mammiferi domestici*, Vol. 4, *Splancnologia. Apparecchio uro-genitale. Feto e i suoi annessi. Peritoneo e topografia addominale*. Edagricole, Milano, Italy.

Baskin LS, Constantinescu SC, Howard PS, McAninch JW, Ewalt DH, Duckett JW, Snyder HM & Macarak EJ (1993). Biochemical characterization and quantitation of the collagenous components of urethral stricture tissue. *J Urol* **150**, 642–647.

Bates AS, Martin RM & Terry TR (2015). Complications following artificial urinary sphincter placement after radical prostatectomy and radiotherapy: a meta-analysis. *BJU Int* **116**, 623–633.

Börgermann C, Kaufmann A, Sperling H, Stöhrer M & Rübben H (2010). The treatment of stress incontinence in men: part 2 of a series of articles on incontinence. *Dtsch Arztebl Int* **107**, 484–491.

Brading AF (1999). The physiology of the mammalian urinary outflow tract. *Exp Physiol* **84**, 215–221.

Brandão S, Parente M, Mascarenhas T, da Silva AR, Ramos I & Jorge RN (2015). Biomechanical study on the bladder neck and urethral positions: simulation of impairment of the pelvic ligaments. *J Biomech* **48**, 217–223.

Braun MH, Sommer F, Haupt G, Mathers MJ, Reifenrath B & Engelmann UH (2003). Lower urinary tract symptoms and erectile dysfunction: co-morbidity or typical "aging male" symptoms? Results of the "Cologne Male Survey". *Eur Urol* **44**, 588–594.

Budras KD, Sack WO & Rock S (2001). *Anatomy of the Horse: an Illustrated Text*, 3rd edn. Iowa State Press, Iowa City, IA, USA.

Carniel EL, Rubini A, Frigo A & Natali AN (2014). Analysis of the biomechanical behaviour of gastrointestinal regions adopting an experimental and computational approach. *Comput Methods Programs Biomed* **113**, 338–345.

Cavalcanti AG, Costa WS, Baskin LS, McAninch JA & Sampaio FJ (2007). A morphometric analysis of bulbar urethral strictures. *BJU Int* **100**, 397–402.

Chung E (2014). A state-of-the-art review on the evolution of urinary sphincter devices for the treatment of post-prostatectomy urinary incontinence: past, present and future innovations. *J Med Eng Technol* **38**, 328–332.

Clark ES, Semrad SD, Bichsel P & Oliver JE (1987). Cystometrography and urethral pressure profiles in healthy horse and pony mares. *Am J Vet Res* **48**, 552–555.

Comiter CV, Sullivan MP & Yalla SV (2003). Correlation among maximal urethral closure pressure, retrograde leak point pressure, and abdominal leak point pressure in men with postprostatectomy stress incontinence. *Urology* **62**, 75–78.

Delancey JO & Ashton-Miller JA (2004). Pathophysiology of adult urinary incontinence. *Gastroenterology* **126**, S23–S32.

Dellmann HD & Eurell JA (1998). *Textbook of Veterinary Histology*, 5th edn. Lippincott Williams & Wilkins, Baltimore, MD, USA.

DuBeau CE (2006). The aging of the lower urinary tract. *J Urol* **175**, S11–S15.

Feng C, Xu YM, Fu Q, Zhu WD, Cui L & Chen J (2010). Evaluation of the biocompatibility and mechanical properties of naturally derived and synthetic scaffolds for urethral reconstruction. *J Biomed Mater Res A* **94**, 317–325.

Fowler FJ, Barry MJ, Lu-Yao G, Roman A, Wasson J & Wennberg JE (1993). Patient-reported complications and follow-up treatment after radical prostatectomy. The National Medicare Experience: 1988–1990 (updated June 1993). *Urology* **42**, 622–629.

Fry CH, Daneshgari F, Thor K, Drake M, Eccles R, Kanai AJ & Birder LA (2010). Animal models and their use in understanding lower urinary tract dysfunction. *Neurourol Urodyn* **29**, 603–608.

Fung YC (1993). *Biomechanics: Mechanical Properties of Living Tissues*, 2nd edn. Springer-Verlag, New York.

Gasser TC, Ogden RW & Holzapfel GA (2006). Hyperelastic modelling of arterial layers with distributed collagen fibre orientations. *J R Soc Interface* **3**, 15–35.

Gregersen H (2003). *Biomechanics of the Gastrointestinal Tract: New Perspectives in Motility Research and Diagnostics.* Springer-Verlag, London.

Griffiths DJ (1971*a*). Hydrodynamics of male micturition. I. Theory of steady flow through elastic-walled tubes. *Med Biol Eng* **9**, 581–588.

Griffiths DJ (1971*b*). Hydrodynamics of male micturition. II. Measurements of stream parameters and urethral elasticity. *Med Biol Eng* **9**, 589–596.

Hached S, Loutochin O, Corcos J, Garon A & Sawan M (2014). Novel, remotely controlled, artificial urinary sphincter: a retro-compatible device. *IEEE-ASME T Mech* **19**, 1352–1362.

Hajivassiliou CA & Finlay IG (1999). Uneven pressure application by the artificial urinary sphincter: an explanation for tissue ischaemia? *BJU Int* **83**, 416–419.

Hampel C, Artibani W, Espuña Pons M, Haab F, Jackson S, Romero J, Gavart S & Papanicolaou S (2004). Understanding the burden of stress urinary incontinence in Europe: a qualitative review of the literature. *Eur Urol* **46**, 15–27.

Hampson LA, McAninch JW & Breyer BN (2014). Male urethral structures and their management. *Nat Rev Urol* **11**, 43–50.

Haworth DJ, Kitta T, Morelli B, Chew DW, Yoshimura N, de Groat WC & Vorp DA (2011). Strain-dependent urethral response. *Neurourol Urodyn* **30**, 1652–1658.

Hoeg HD, Slatkin AB, Burdick JW & Grundfest WS (2000). Biomechanical modeling of the small intestine as required for the design and operation of a robotic endoscope. *P IEEE Int Conf Robot* **2**, 1599–1606.

Holzapfel GA (2000). *Nonlinear Solid Mechanics: a Continuum Approach for Engineering.* J. Wiley & Sons Ltd, New York, NY, USA.

Idzenga T, Pel JMJ & van Mastrigt R (2006). A biophysical model of the male urethra: comparing viscoelastic properties of polyvinyl alcohol urethras to male pig urethras. *Neurourol Urodynam* **25**, 451–460.

Irwin DE, Milsom I, Hunskaar S, Reilly K, Kopp Z, Herschorn S, Coyne K, Kelleher C, Hampel C, Artibani W & Abrams P (2006). Population-based survey of urinary incontinence, overactive bladder, and other lower urinary tract symptoms in five countries: results of the EPIC study. *Eur Urol* **50**, 1306–1315.

Ishii T, Kambara Y, Yamanishi T & Naya Y (2014). Urine flow dynamics through prostatic urethra with tubular organ modeling using endoscopic imagery. *IEEE J Transl Eng Health Med* **2**, 1800709.

Joller D, Mushkolaj S, Ratia-Garcia J, Marti F, Bachmann A & Müller B (2012). Minipig urethra: a suitable animal model in vitro. *Technol Health Care* **20**, 329–336.

König HE & Liebich HG (2009). *Veterinary Anatomy of Domestic Mammals: Textbook and Colour Atlas.* Schattauer, Stuttgart, Germany.

Lalla M, Danielsen CC, Austevoll H, Olsen LH & Jørgensen TM (2007). Biomechanical and biochemical assessment of properties of the anterior urethra after hypospadias repair in a rabbit model. *J Urol* **177**, 2375–2380.

Lecamwasam HS, Sullivan MP, Yalla SV & Cravalho EG (1999). The flow regimes and the pressure-flow relationship in the canine urethra. *Neurourol Urodyn* **18**, 521–541.

Maia RS, Babinski MA, Figueiredo MA, Chagas MA, Costa WS & Sampaio FJ (2006). Concentration of elastic system fibers in the corpus cavernosum, corpus spongiosum, and tunica albuginea in the rabbit penis. *Int J Impot Res* **18**, 121–125.

McVary K (2006). Lower urinary tract symptoms and sexual dysfunction: epidemiology and pathophysiology. *BJU Int* **97**, 23–28.

Marti F, Leippold T, John H, Blunschi N & Müller B (2006). Optimization of the artificial urinary sphincter: modelling and experimental validation. *Phys Med Biol* **51**, 1361–1375.

Mijailovich SM, Sullivan MP, Yalla SV & Venegas JG (2007). Effect of urethral compliance on the steady state p-Q relationships assessed with a mechanical analog of the male lower urinary tract. *Neurourol Urodyn* **26**, 234–246.

Minassian VA, Drutz HP & Al-Badr A (2003). Urinary incontinence as a worldwide problem. *Int J Gynecol Obstet* **82**, 327–338.

Montague DK, Angermeier KW & Paolone DR (2001). Long-term continence and patient satisfaction after artificial sphincter implantation for urinary incontinence after prostatectomy. *J Urol* **166**, 547–549.

Müller B, Schulz G, Herzen J, Mushkolaj S, Bormann T, Beckmann F & Püschel K (2010). Morphology of urethral tissues. *Proc SPIE* **7804**, 78040D1–78040D12.

Mundy AR & Andrich DE (2011). Urethral strictures. *BJU Int* **107**, 6–26.

Nagatomi J, Gloeckner DC, Chancellor MB, DeGroat WC & Sacks MS (2004). Changes in the biaxial viscoelastic response of the urinary bladder following spinal cord injury. *Ann Biomed Eng* **32**, 1409–1419.

Natali AN, Carniel EL & Gregersen H (2009). Biomechanical behaviour of oesophageal tissues: material and structural configuration, experimental data and constitutive analysis. *Med Eng Phys* **31**, 1056–1062.

Neuhaus J, Dorschner W, Mondry J & Stolzenburg JU (2001). Comparative anatomy of the male guinea-pig and human lower urinary tract: histomorphology and three-dimensional reconstruction. *Anat Histol Embryol* **30**, 185–192.

Nitti VW (2001). The prevalence of urinary incontinence. *Rev Urol* **3**, S2–S6.

Nozaki K (1959). On histology and nerve supply of urethra, prostata and gl. bulbourethralis in flying-squirrel. *Arch Histol Japon* **17**, 23–44.

Peng Y, Khavari R, Nakib NA, Boone TB & Zhang Y (2015*a*). Assessment of urethral support using MRI-derived computational modeling of the female pelvis. *Int Urogynecol J* **27**, 205–212.

Peng Y, Khavari R, Nakib NA, Stewart JN, Boone TB & Zhang Y (2015*b*). The single-incision sling to treat female stress urinary incontinence: a dynamic computational study of outcomes and risk factors. *J Biomech Eng* **137**, 091007-1–091007-7.

Pozor MA & McDonnell SM (2002). Ultrasonographic measurements of accessory sex glands, ampullae, and urethra of normal stallions of various size types. *Theriogenology* **58**, 1425–1433.

Prantil RL, Jankowski RJ, Kaiho Y, de Groat WC, Chancellor MB, Yoshimura N & Vorp DA (2007). Ex vivo biomechanical properties of the female urethra in a rat model of birth trauma. *Am J Physiol Renal Physiol* **292**, F1229–F1237.

Ramesh MV, Raj D, Sanjeevan Kalavampra V & Dilraj N (2014). Design of wireless real time artificial sphincter control system for urinary incontinence. *IEEE Int Symp Technology Management and Emerging Technologies (ISTMET)*, Bandung, Indonesia, 44–49.

Ronen N (1994). Measurements of urethral pressure profiles in the male horse. *Equine Vet J* **26**, 55–58.

Rosen R, Altwein J, Boyle P, Kirby RS, Lukacs B, Meuleman E, O'Leary MP, Puppo P, Robertson C & Giuliano F (2003). Lower urinary tract symptoms and male sexual dysfunction: the multinational survey of the aging male (MSAM-7). *Eur Urol* **44**, 637–649.

Salinas J, Virseda M, Fuente MP, Mellado F & Uson AC (1992). A study on the viscoelastic properties of the urinary bladder in dogs. *Urol Int* **49**, 185–190.

Singla N, Siegel JA, Simhan J, Tausch TJ, Klein A, Thoreson GR & Morey AF (2015). Does pressure regulating balloon location make a difference in functional outcomes of artificial urinary sphincter? *J Urol* **194**, 202–206.

Spirka T, Kenton K, Brubaker L & Damaser MS (2013). Effect of material properties on predicted vesical pressure during a cough in a simplified computational model of the bladder and urethra. *Ann Biomed Eng* **41**, 185–194.

Thind P (1995). An analysis of urethral viscoelasticity with particular reference to the sphincter function in healthy women. *Int Urogynecol J* **6**, 209–228.

Thüroff JW, Abrams P, Andersson KE, Artibani W, Chapple CR, Drake MJ, Hampel C, Neisius A, Schröder A & Tubaro A (2011). EAU Guidelines on Urinary Incontinence. *Eur Urol* **59**, 387–400.

Todros S, Pavan P & Natali AN (2015). Biomechanical properties of synthetic surgical meshes for pelvic prolapse repair. *J Mech Behav Biomed* **55**, 271–285.

Tziannaros M, Glavin SE & Smith FT (2013). Three-dimensional effects in the lower urinary tract. *IMA J Appl Math* **78**, 729–749.

Van Kerrebroeck PE, Koldewijn EL, Scherpenhuizen S & Debruyne FM (1993). The morbidity due to lower urinary tract function in spinal cord injury patients. *Paraplegia* **31**, 320–329.

Van Mastrigt R & Nagtegaal JC (1981). Dependence of the viscoelastic response of the urinary bladder wall on strain rate. *Med Biol Eng Comput* **19**, 291–296.

Weiss JA & Gardiner JC (2001). Computational modeling of ligament mechanics. *Crit Rev Biomed Eng* **29**, 1–70.

Wolfe DF & Moll HD (1999). *Large Animal Urogenital Surgery*. Williams & Wilkins, Baltimore, MD, USA.

Wu Y, Zhang SX, Luo N, Qiu MG, Tan LW, Li QY, Liu GJ & Li K (2010). Creation of the digital three-dimensional model of the prostate and its adjacent structures based on Chinese visible human. *Surg Radiol Anat* **32**, 629–635.

Additional information

Competing interests

None declared.

Author contributions

A.N.N. planned and critically revised the research activities. G.M.D.B., Y.A., E.L.C. and A.F. were involved in preparation and collection of urethral samples. L.C., Y.A., E.L.C. and A.F. developed the histological analysis. P.G.P., S.T. and P.P. developed the mechanical tests on urethral tissues. E.L.C., A.F., C.G.F., A.R. and Y.A. developed the mechanical tests on urethral structures. E.L.C., A.F., C.G.F. and P.P. developed postprocessing of experimental data, model interpolation and critical review of results. A.N.N., P.G.P. and S.T. critically revised the manuscript for intellectual content. All authors have approved the final version of the manuscript and agree to be accountable for all aspects of the work. All persons designated as authors qualify for authorship, and all those who qualify for authorship are listed.

Funding

This study has been supported by the University of Padova, project no. CPDA148900/14, entitled 'COMPUR: Definition of COMPutational tools for the analysis of the biomechanical functionality of the lower URinary system'.